Accepted by ApJ Letters 24 December 2009
Preprint typeset using LaTeX style emulateapj v. 11/10/09

arXiv:1001.0276v1 [astro-ph.CO] 2 Jan 2010

THE GALAXY-WIDE DISTRIBUTIONS OF MEAN ELECTRON DENSITY IN THE HII REGIONS OF M51 AND NGC 4449.

Leonel Gutiérrez[1,2] and John E. Beckman[2,3]

Accepted by ApJ Letters 24 December 2009

ABSTRACT

Using ACS-HST images to yield continuum subtracted photometric maps in Hα of the Sbc galaxy M51 and the dwarf irregular galaxy NGC 4449, we produced extensive (over 2000 regions for M51, over 200 regions for NGC4449) catalogues of parameters of their HII regions: their Hα luminosities, equivalent radii and coordinates with respect to the galaxy centers. From these data we derived, for each region, its mean luminosity weighted electron density, $\langle n_e \rangle$, determined from the Hα luminosity and the radius, R, of the region. Plotting these densities against the radii of the regions we find excellent fits for $\langle n_e \rangle$ varying as $R^{-1/2}$. This relatively simple relation has not, as far as we know, been predicted from models of HII region structure, and should be useful in constraining future models. Plotting the densities against the galactocentric radii, r, of the regions we find good exponential fits, with scale lengths of close to 10 kpc for both galaxies. These values are comparable to the scale lengths of the HI column densities for both galaxies, although their optical structures, related to their stellar components are very different. This result indicates that to a first approximation the HII regions can be considered in pressure equilibrium with their surroundings. We also plot the electron density of the HII regions across the spiral arms of M51, showing an envelope which peaks along the ridge lines of the arms.

Subject headings: ISM: general — HII regions — galaxies: structure

1. INTRODUCTION

Electron densities for HII regions can be measured in two different ways, which respectively yield two different ranges of values. Density sensitive emission line ratios, such as the [SII] $\lambda\lambda$6731/6716Å doublet ratio, or the [OII] $\lambda\lambda$3729/3726Å doublet ratio give values in the range of hundreds (Zaritsky et al. 1994; McCall et al. 1985). However measurements using Hα surface brightness to derive the emission measure, together with the estimated radius of an HII region, give values in the range 1-10 (see e.g. Rozas et al. 1996). This type of dichotomy was recognized long ago by Osterbrock & Flather (1959) who used the emission line ratio of the [OII] doublet, $\lambda\lambda$3729/3726Å, as their version of the first technique, and cm wavelength radio emission (from the literature) to estimate the emission measure, i.e. for the second technique. They reached the conclusion that the best way to reconcile the differences, of more than an order of magnitude between the two techniques, is to assume that the emission nebula is clumpy, with dense clouds embedded in a much more tenuous substrate. The line ratios are strongly weighted by density, and yield values reflecting the densities of the dense clumps, while the electron density derived using the emission measure and the overall size of the HII region is a geometrical average, whose balance between the contribution of the clumps and the substrate depends on the fractional volume occupied by the former. In models for HII regions based on recognition of this inhomogeneity, the fractional volume occupied by the clumps is termed the filling factor, and a first order approximation can be made that the interclump substrate makes a negligible contribution to the line emission, so that the interclump volume can be considered to have negligible electron density (see Osterbrock (1989) for a standard treatment). In the present article we are using the measured luminosities of HII regions in Hα to compute an electron density using the second method, so our values are to be taken as the means produced by the second technique. We will use them to derive comparative electron densities of selected HII regions in M51 and NGC 4449, to establish functional relations between them, the sizes of the HII regions, and their positions within the discs of their respective galaxies, and hence to provide an overview of the global behavior of the electron density within the discs of the two galaxies.

2. THE OBSERVATIONAL DATA AND ITS TREATMENT

M51 was observed in January 2005 with the ACS on HST using the broad band filters F435W (close to the standard B band) F555W (close to V) and F814W (close to I) and the narrow band filter F658N (Hα) within observational program 10452 (P.I. S. Beckwith, Hubble Heritage Team). The data used here were corrected, calibrated, and combined into a mosaic of the galaxy by Mutchler et al. (2005). The images of NGC 4449 were also taken with the ACS, through the same filters as those used for M51, in November 2005, within program GO 10585 (P.I. A. Aloisi). The images were taken at two different positions along the major axis of the galaxy, with four dithered pointings on each position (Annibali et al. 2008) to help cosmic ray removal. We combined them using MULTIDRIZZLE (Koekemoer et al. 2002), yielding overall exposure times

---

leonel@astrosen.unam.mx, jeb@iac.es
[1] Universidad Nacional Autónoma de México, Instituto de Astronomía, Ensenada, B. C. México
[2] Instituto de Astrofísica de Canarias, C/ Via Láctea s/n, 38200 La Laguna, Tenerife, Spain
[3] Consejo Superior de Investigaciones Científicas, Spain

of 3600s, 2400s, 2000s and 360s respectively for the four named filters. The total resulting field is sized 345×200 arcsec^2; we produced mosaics containing complete images of the galaxy in all bands.

For both galaxies standard correction and calibration procedures were used (bias, flat-field, dark current, and distortion corrections) using the ACS pipeline calibration suite CALACS (Hack et al 2000). Use of the Multidrizzle process allowed us to correct for detector defects and distortions, though we retained the original pixel scales (0.05 arcsec per pixel). After this process we converted the images from e-/s to flux in erg cm^{-2} s^{-1} Å^{-1} using the standard PHOTOFLAM conversion factor (Sirianni et al. 2005). We aligned the continuum and Hα images and produced a continuum subtracted Hα image, after deriving the factor of proportionality between the continuum in the on-band and off-band filters, following the method of Böker et al. (1999). A more detailed description of our image treatment can be found in Gutiérrez et al. (2010, in preparation). The method for measuring the Hα flux of an HII region requires defining its boundaries in the presence of any local diffuse Hα emission and any overlapping neighbour regions, using circular or rectangular defining apertures. The boundary of an HII region is defined as containing only pixels whose brightness is greater than 3σ, measured on the background. For NGC 4449 the diffuse background subtraction presented special difficulties due to its strength, and to perform this accurately we used a selective filter, as defined in Gutiérrez et al. (2010, in preparation). Once a local background brightness was determined, it was multiplied by the number of pixels within the HII region and subtracted from the flux directly measured within the region, to yield the measured flux from the region. To allow for the overlap of regions, if the brightness between the two maxima falls below 2/3 of the value of the fainter maximum we considered them to be two separate regions, with the boundary in the depression of the brightness distribution. Where this criterion was not met we classified the region as single.

To allow for the contribution of the [NII] doublet through the F658N filter, for M51 we used the mean of the observed ratios of these lines to Hα for 10 HII regions in that galaxy by Bresolin et al. (2004), which show very limited variations from region to region, to calculate the factor by which the observed flux should be reduced, using the filter transmission curve and the observed redshift of M51. For NGC 4449 we used the observed ratio from Kennicutt (1992). The factor for M51 was 0.67, and the corresponding factor for NGC 4449 is 0.86. We understand that radial decline in metallicity (especially in M51), will give rise to errors in using these blanket numbers for each object, but we can show that these errors are of second order (Gutiérrez et al. 2010, in preparation). Also, we estimated the possible systematic error due to the presence of the [OIII] emisison line at λ5007Å in the F555W filter and found this to be less than 1%.

Finally, in deriving absolute fluxes we took the distance to M51 as 8.39 Mpc, following Feldmeier et al. (1997) and the distance to NGC 4449 as 3.82 Mpc, following Annibali et al. (2008). We measured the luminosity of each region as outlined above, and also, from the continuum- and background-subtracted Hα image, determined the area subtended by the image, and derived a value for an equivalent radius, obtained dividing the area by π and taking the square root. With these measurements we could determine a mean electron density for a each region, as described below. A catalogue of 2657 regions of M51, and 273 regions of NGC4449 was produced, containing positions, measured fluxes and luminosities in Hα, and equivalent radii (see Gutiérrez et al. 2010 for details).

3. THE MEAN ELECTRON DENSITY OF THE HII REGIONS

3.1. *Electron density as a function of HII region radius*

We described in the introduction the inhomogeneity of HII regions, but with the set of observations described here we confine our attention to the mean electron density ($\langle n_e \rangle$), and use the "Case B" formula (Osterbrock 1989)

$$\langle n_e \rangle = \sqrt{\frac{2.2L(H\alpha)}{\frac{4}{3}\pi\alpha_B h\nu_{H\alpha}R^3}} \tag{1}$$

to derive this, where L(Hα) is the Hα luminosity, α_B is the case B recombination coefficient, $h\nu_{H\alpha}$ is the energy of an Hα photon, and R is the equivalent radius of the HII region. If we measure R in pc and L(Hα) in erg s^{-1}, and taking a canonical value for the temperature of 10000 K we can rewrite equation 1 as

$$\langle n_e \rangle = 1.5 \times 10^{-16}\sqrt{\frac{L(H\alpha)}{R^3}}cm^{-3}. \tag{2}$$

In Fig. 1 we show the mean electron densities of all the regions observed in M51 against their equivalent radii. There is considerable scatter, which we will investigate further below. A linear fit to the points gives the result:

$$\langle n_e \rangle = \frac{28.9}{R^{0.56}}; \tag{3}$$

in qualitative terms, the larger regions have lower mean electron densities. The functional trend is quite well reproduced by the HII regions in NGC 4449 as we can see in Fig. 2. With far fewer points, the best linear fit is given by

$$\langle n_e \rangle = \frac{44.2}{R^{0.45}}. \tag{4}$$

These are only two galaxies, but the trends can at this stage be usefully summarized by the simple expression

$$\langle n_e \rangle \sim \frac{1}{R^{0.5}}. \tag{5}$$

This relation is obeyed more closely for both galaxies if we correct the relationship between $\langle n_e \rangle$ and R for the dependence of $\langle n_e \rangle$ on the galactocentric radius, r, as described in section 3.2 below. Making this correction gives adjusted values of -0.52, and -0.47 for the exponents in M51 and NGC 4449, respectively.

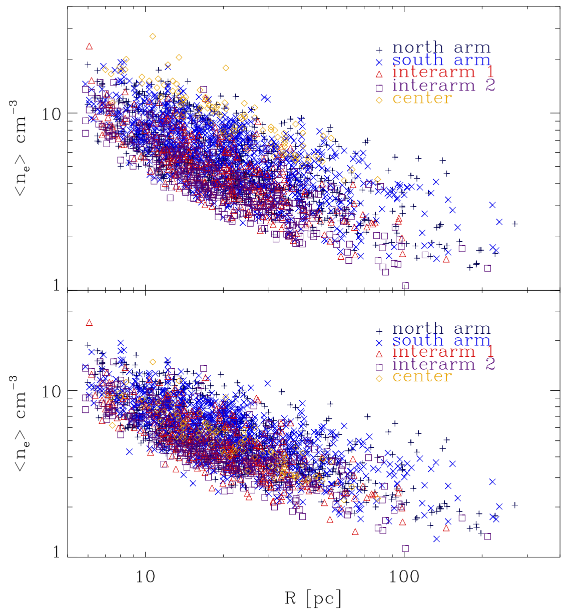

FIG. 1.— Mean electron densities of all the HII regions measured in M51 as a function of equivalent radius. In the lower panel the densities have been corrected by a factor which takes into account their galactocentric distances (plotted in Fig. 3).

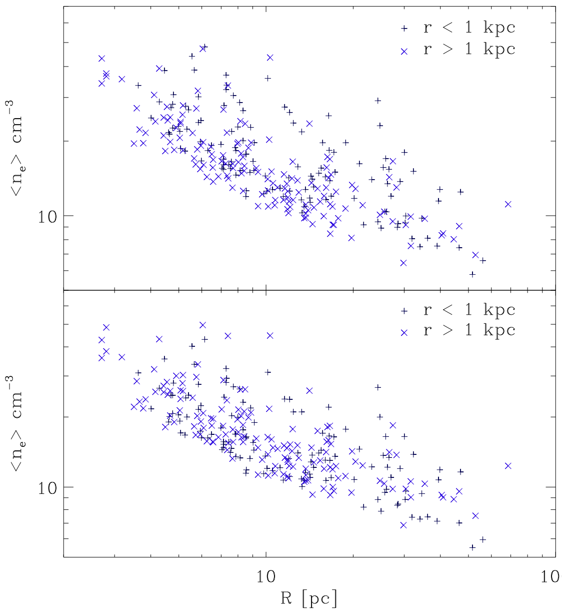

FIG. 2.— Mean electron densities of the HI regions measured in NGC 4449 as a function of equivalent radius. In the lower panel the densities have been corrected by a factor which takes into account their galactocentric distances (plotted in Fig. 4).

3.2. *Electron density as a function of galactocentric distance*

In the upper panel of Fig. 3 we have plotted the mean electron density, $\langle n_e \rangle$, against galactocentric radius, r, for M51, including all the regions, but distinguishing by point styles among those found in different large scale features of the galaxy: arms, interarm zones, and the central kpc. The outstanding feature of this plot is the single straight line fit (which is an exponential, as the electron density scale is logarithmic), which has the form:

$$\langle n_e \rangle = \langle n_e \rangle_o \, e^{-r/h}, \qquad (6)$$

where $\langle n_e \rangle_o$, with value 10±1 cm^{-3} is a central value of electron density and h is a scale length, which takes the value 10±1.0 kpc. We have limited the fit to galactocentric radii within $r = 10.4$ kpc, because beyond this radius there is an abrupt local rise and fall in $\langle n_e \rangle$, attributable to the effect of the interacting neighbour galaxy NGC 5195. We can make separate estimates for the constants $\langle n_e \rangle_o$ and h in the arms and in the interarm zones. For the arms this gives us $\langle n_e \rangle_o = 10$ cm^{-3} and $h = 11$ kpc, while for the interarm zones we find $\langle n_e \rangle_o = 8$ cm^{-3}, and $h = 11$ kpc .

Since we know that in the upper panel of Fig. 3 much of the apparent scatter is due to the (inverse) dependence of $\langle n_e \rangle$ on the radii of the individual HII regions, we next opted to apply a normalized correction factor for this effect to all the data, and replot the figure, yielding the central panel of Fig. 3, in which the (exponential) linear fit is clearly much improved. To make the fit we have chosen to leave out the zones from 1.4 to 4.6 kpc from the center, and from 10.4 to 11.5 kpc from the center, and now find values of $\langle n_e \rangle_o$ and h of 12 cm^{-3} and 9 kpc respectively. It is notable that the scale length found for the neutral atomic hydrogen component of M51 by Tilanus & Allen (1991) is 9.1 kpc, on which we will comment further below. We should point out that the zone between the center of the galaxy and a radius of 1.4 kpc does fit the exponential for the disc as a whole.

To take a look at the global behavior we have taken averages of all the regions within annuli of width 200 pc and have plotted, in the lower panel of Fig. 3 these values against galactocentric radius. This shows the overall trend in $\langle n_e \rangle$, and we can pick out the general decline with radius, but note a plateau between 1.4 kpc and 4.6 kpc. If we omit the points in this interval from those entering the exponential fit, we obtain values for $\langle n_e \rangle_o$ and h, of 11 cm^{-3} and 9 kpc respectively.

To compute the effect of the temperature gradient on the determination of $\langle n_e \rangle$ and of its gradient, we used data from Bresolin et al. (2004) giving the O abundance gradient, and the widely used CLOUDY model (Ferland et al. 1998) to derive the effective temperature gradient, which we then incorporated into the expression

$$\langle n_e \rangle = 2.3 \times 10^{-18} \sqrt{\frac{L(H\alpha)\, T^{0.91}}{R^3}} cm^{-3}, \qquad (7)$$

and recalculated the electron densities. This introduced a change in the exponent of the relation between $\langle n_e \rangle$ and radius from -0.56 to -0.55, and in the scale length from 9.2 to 9.9 kpc. These are the values represented in Fig. 3.

Here we should point out the similarity of the lower panel of Fig. 3 with the radial plot of the azimuthally averaged HI column density in Tilanus & Allen (1991).

General expressions for $\langle n_e \rangle$ are then:

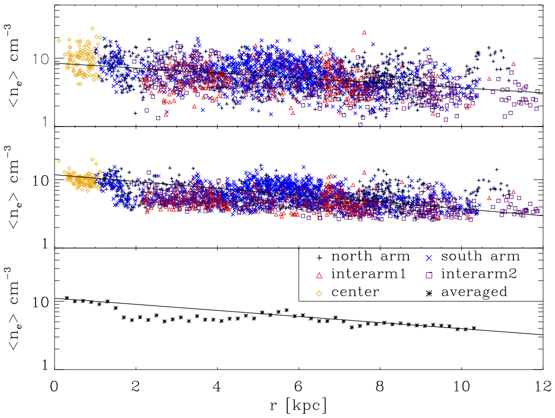

FIG. 3.— Mean electron density ($\langle n_e \rangle$) vs galactocentric radius, r, for M51, distinguishing by the point styles those found in the arms, in the interarm zones, and within the central kpc. The points in the centre panel were found by applying a normalized correction factor to those in the upper panel, in order to take into account the variation of $\langle n_e \rangle$ with region radius, R. In the lower panel we show the result of taking the median value of $\langle n_e \rangle$ for the full sample of regiones within annuli of width 200 pc.

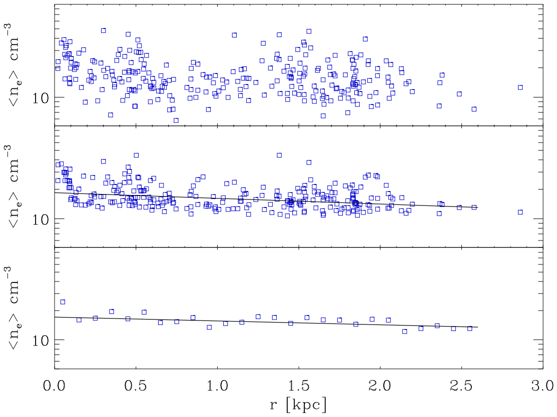

FIG. 4.— Mean electron densities ($\langle n_e \rangle$) for the measured HI regions NGC 4449. In the upper panel $\langle n_e \rangle$ is plotted against galactocentric radius, in the centre panel $\langle n_e \rangle$ has been modified by a correction factor to take into account the variation with the radii R of the individual regions (a $1/R^{0.5}$ dependence), and in the lower panel we plot the median values of all the regions sampled within annuli of 100 pc width.

$$\langle n_e \rangle = \begin{cases} 45.8\ e^{-r/10}\ R^{-0.55} cm^{-3}; \\ \qquad\qquad r < 1.4 \text{ kpc } \& \ r > 4.6 \text{ kpc} \\ 28.9\ R^{-0.55} cm^{-3}; \\ \qquad\qquad r \in [1.4, 4.6] \text{ kpc}. \end{cases} \tag{8}$$

The results for NGC 4449 are summarized in Fig. 4. In the upper panel of Fig. 4 we have plotted $\langle n_e \rangle$ against galactocentric radius for all our measured regions, in the central panel we present the data normalized to take into account the $1/R^{0.5}$ relation explained above, while in the lower panel we have averaged the points in the central panel in annuli of width 200 pc. In the latter two panels the linear fits show the exponential radial decline in mean electron density, which is fitted by the whole galaxy outside the central 120 pc. Using the best fit in the lower panel of Fig. 4 and normalizing, $\langle n_e \rangle$ is given by:

$$\langle n_e \rangle = 45.7\ e^{-r/11}\ R^{-0.45}. \tag{9}$$

This scale length here is 11 kpc which is much bigger than the optical radius of the galaxy. However, Hunter et al (1998) observed an HI disc with a central dense component some 4.5 kpc in radius embedded in a much larger elliptical component with a major axis limiting radius of 18 kpc. Taken our cue from M51, which has an HI scale length of 9 kpc and a limiting HI radius of 15 kpc (Meijerink et al. 2005), we can claim here that the HII region scale length and the HI scale length of NGC 4449 are comparable, consistent with the scenario where the electron densities in the HII regions follow the column density of the HI gas, as in M51.

3.3. *The mean electron density as a function of position in the spiral arms of M51*

Finally in this section we show in Fig. 5 the electron density in the spiral arms of M51 as a function of the position relative to the central ridge line of the arms. The ridge lines of the arms, used to define this relative position, were measured using the continuum image through the F814W filter. The abscissa in these plots is the distance from the ridge line to the regions. We can see that the mean electron density reaches peak values along the ridge line, which is not surprising, but taking the complete populations of HII regions we can see that the systematic increase of density towards the ridge line is a property of the upper envelopes of the plots for the two arms. There are many regions close to the ridge line with relatively low densities, though no high density regions towards the edges of the arms.

4. CONCLUSIONS

We have used the Hα luminosities and measured radii of the populations of HII regions in M51 and NGC 4449, from HST images, to derive their mean electron densities, aware that their inhomogeneous structures imply that the mean electron density does not describe either the in situ densities of their strongly emitting clumps, or the densities of their more tenuous interclump gas, but is a luminosity weighted mean over the HII region volume. We have found two functional dependences of this mean electron density parameter, valid for both galaxies: it varies inversely proportionally to the square root of the radius of an HII region, and it falls exponentially with galactocentric radius. The former relation must depend on the effects of the energy outflow from the massive ionizing stars on their environment. As far as we are aware it does not correspond to the predictions of any previously published specific model (Scoville et al. (2001) show a graph for M51 which could be used to infer a similar result, but did not derive an explicit relation for these variables), and sets interesting constraints on the physics of OB cluster formation and the subsequent interaction with the cluster environment. The latter relation, with the scale length for the electron density

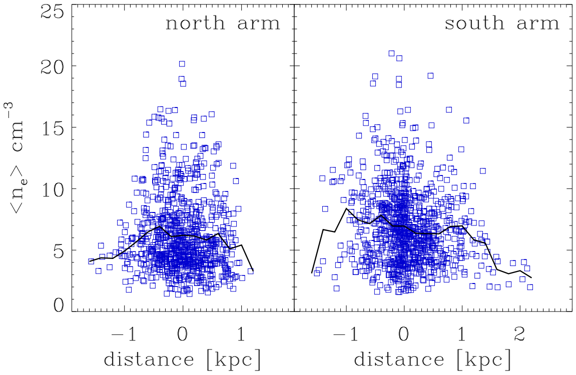

FIG. 5.— The mean electron densities of the HII regions in M51 plotted against distance from the central ridge line of the arms in M51 (squares). Also shown is the variation of the average value in 200 pc bins of these densities as a function of this distance (thick lines) for both arms.

comparable with that for the HI column density in galaxies of very different sizes and types (M51 is a Sbc while NGC 4449 is an IBm), demonstrates that, globally, an HII region is in quasi-pressure equilibrium with its surrounding gas. The quantitative differences between the density of arm and interarm regions are not great, but also reflect this quasi-equilibrium, since the values are systematically somewhat lower for the interarm regions. Finally the distribution of mean electron densities across a spiral arm has an upper envelope peaking along the center, the ridge line of the arm, but values well below the envelope are distributed fairly uniformly across the arm. These relations should be of value for improving physical descriptions of HII regions as zones of interac-

REFERENCES

Annibali, F., Aloisi, A., Mack, J., et al. 2008, AJ 135, 1900

Böker. T., Calzetti, D., Sparks, W., et al. 1999, ApJS 124, 95

Bresolin, F., Garnett, D. R., & Kennicutt, R. C. 2004, ApJ 615, 228

Feldmeier J. J., Ciardullo R., & Jacoby G. H. 1997, ApJ 479, 231

Ferland, G. J., Korista, K. T., Verner, D. A., Ferguson, J. W., Kingdon, J.B., & Verner, E. M. 1998, PASP, 110, 761

Hack W.J., & Greenfield, P. 2000, *ASP Conf. Ser., Vol. 216, Astronomical Data Analysis Software and Systems IX*, eds. N. Manset, C. Veillet, & D. Crabtree (San Francisco: ASP), 433

Hunter, D. A., Wilcots, E. M., van Woerden, H., Gallagher, J. S., & Kohle, S. 1998, ApJL 495, 47

Kennicutt, R. C. 1992, ApJ 388, 310

Koekemoer, A. M., Fruchter, A. S., Hook, R. N., & Hack, W. 2002, HST Calibration Workshop, Ed. S. Arribas, A. M. Koekemoer, B. Whitmore (STScI: Baltimore), 337. In http://www.stsci.edu/

McCall, M. L., Rybski, P. M., & Shields, G. A. 1985, ApJS 57, 1

Meijerink, R., Tilanus, R. P. J., Dullemond, C. P., Israel, F. P., & van der Werf, P. P. 2005, A&A, 430, 427

Mutchler, M., Beckwith, S.V.W., Bond, H. E., Christian, C., Frattare, L., Hamilton, F., Hamilton, M., Levay, Z., Noll, K., & Royle, T. 2005, "Hubble Space Telescope multi-color ACS mosaic of M51, the Whirlpool Galaxy", Bulletin of the American Astronomical Society, Vol.37, No.2. http://www.aas.org/publications/baas/v37n2/ aas206/339.htm

Osterbrock, D. 1989, in *Astrophysics of Gaseous Nebulae and Active Galactic Nuclei*, Mill Valley: University Science Books

Osterbrock, D. & Flather, E. 1959, ApJ 129, 260

Rozas, M., Knapen, J. H., & Beckman, J. E. 1996, A&A 312, 275

Scoville, N. Z., Polletta, M., Ewald, S., Stolovy, S. R., Thompson, R., & Rieke, M. 2001, AJ 122, 3017

Sirianni, M., Jee, M. J., Benítez, N., et al. 2005, PASP 117, 1049

Tilanus, R. P. J. & Allen, R. J. 1991, A&A 244, 8

Zaritsky, D., Kennicutt, R. C. Jr., & Huchra, J. P. 1994, ApJ 420, 87